Journal of Hydrology xxx (2009) xxx–xxx

Contents lists available at ScienceDirect

Journal of Hydrology

journal homepage: www.elsevier.com/locate/jhydrol

Assessment of a distributed biosphere hydrological model against streamflow and MODIS land surface temperature in the upper Tone River Basin

Lei Wang [a,*], Toshio Koike [a], Kun Yang [b], Pat Jen-Feng Yeh [c]

[a] Department of Civil Engineering, The University of Tokyo, Bunkyo-ku, Tokyo 113-8656, Japan
[b] Institute of Tibetan Plateau Research, Chinese Academy of Sciences, Beijing 100085, China
[c] Institute of Industrial Science, The University of Tokyo, Tokyo 153-8505, Japan

ARTICLE INFO

Article history:
Received 19 August 2008
Received in revised form 24 June 2009
Accepted 2 August 2009
Available online xxxx

This manuscript was handled by K. Georgakakos, Editor-in-Chief, with the assistance of Christa D. Peters-Lidard, Associate Editor

Keywords:
Distributed biosphere hydrological model
Water cycle
Energy budget
Land surface temperature
Streamflow
Flood

SUMMARY

Land surface temperature (LST) is a key parameter in land–atmosphere interactions. The recently released Moderate Resolution Imaging Spectroradiometers (MODIS) LST Version 5 products have provided good tools to evaluate water and energy budget modelling for river basins. In this study, a distributed biosphere hydrological model (WEB-DHM; so-called water and energy budget-based distributed hydrological model) that couples a biosphere scheme (SiB2) with a geomorphology-based hydrological model (GBHM), is applied to the upper Tone River Basin where flux observations are not available. The model facilitates a better understanding of the water and energy cycles in this region. After being calibrated with discharge data, WEB-DHM is assessed against observed streamflows at four major gauges and MODIS LST. Results show that long-term streamflows including annual largest floods are well reproduced. As well, both daytime and nighttime LSTs simulated by WEB-DHM agree well with MODIS observations for both basin-averaged values and spatial patterns. The validated model is then used to analyze water and energy cycles of the upper Tone River Basin. It was found that from May to October, with relatively large leaf area index (LAI) values, the simulated daily maximum LST is close to soil surface temperature (T_g) since T_g is much greater than canopy temperature (T_c) in their peak values; while the daily minimum LST appears similar to T_c. For other months with relatively small LAI values, the diurnal cycles of LST closely follow T_g.

Introduction

The Tone River Basin is Japan's largest with a catchment area of 15,628.7 km^2. It is the main water supply for about 27 million people living in the Kanto region, which includes the Tokyo Metropolitan Area, the political and economic center of Japan.

The upper Tone River Basin, lying upstream of the Maebashi hydrological station (see Fig. 1), was selected for this study because datasets were available. The target basin locates northwest of Tokyo (see Fig. 1), and is at longitude from 138.38°E′ to 139.43°E′ and latitude from 36.36°N′ to 37.06°N′. The catchment area studied is about 3300 km^2. Long-term mean precipitation in this region is about 1500 mm per year. Heavy rainfall events occurring from June to October are commonly associated with typhoons and Mei-yu front activities, leading to high flood risks in the lower regions. Several reservoirs have been constructed in the upper mountainous regions to protect the Lower Kanto plain from flooding (see Fig. 1). Details of these reservoirs can be found in Yang et al. (2004).

Because of a previous lack of heat flux observations, there has been no previous study with energy-related analyses for this region. However, water and energy intrinsically interact with each other through evapotranspiration (or latent heat flux), which comprises evaporation from the soil surface, and evaporation from canopy interceptions as well as transpiration from the vegetation canopy. In a basin-scale hydrological simulation, evapotranspiration (ET) has an important role in determining both long-term water budgets and short-term flood events. First, ET determines the partition from precipitation to runoff and ET from monthly to longer timescales. Second, the accurate estimation of ET in an earlier simulation is crucial to obtain initial soil moisture conditions for flood event simulation, especially in dry conditions. Therefore, to improve both water budget studies and flood predictions for the region, it is important that the energy budget be investigated to improve our understanding of the water and energy cycles that are coupled in a basin.

In last 20 years, a few spatially-distributed hydrological models with coupled water and energy budgets (e.g., Wigmosta et al., 1994; Famiglietti and Wood, 1994; Peters-Lidard et al., 1997;

* Corresponding author. Address: River Lab, Department of Civil Engineering, The University of Tokyo, Hongo 7-3-1, Bunkyo-ku, Tokyo 113-8656, Japan. Tel.: +81 3 5841 6107; fax: +81 3 5841 6130.
E-mail address: wang@hydra.t.u-tokyo.ac.jp (L. Wang).

0022-1694/$ - see front matter © 2009 Elsevier B.V. All rights reserved.
doi:10.1016/j.jhydrol.2009.08.005

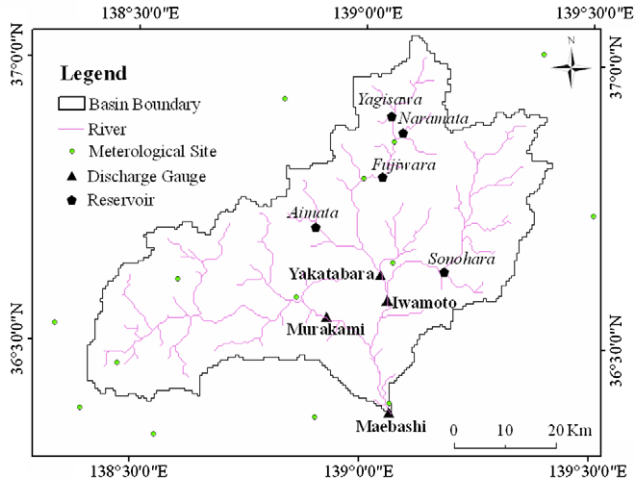

Fig. 1. The upper Tone River Basin.

Rigon et al., 2006; Bertoldi et al., 2006; Tang et al., 2006) have been developed and largely improved the basin-scale water and energy budget studies. These models have been evaluated with observed discharges; however, it is rather difficult to evaluate these models' performance in representing basin-scale energy cycles, because observations of spatially variable energy fluxes with high resolutions are presently not available over large regions.

Satellite remote sensing offered the most feasible, consistent, and accurate means of providing global fields of land surface parameters (Sellers et al., 1997). In recent years, Moderate Resolution Imaging Spectroradiometers (MODIS) datasets with global coverage and high resolution, were widely used for model evaluations in geophysical studies (e.g., Turner et al., 2003; Brown et al., 2008; Parajka and Bloeschl, 2008; Twine and Kucharik, 2008; Sheng et al., 2009). The newly-released MODIS land surface temperature (LST) Version 5 (V5) products (Wan, 2008) provide us an opportunity to improve water and energy budget studies in basin scales, because LST is one of the crucial parameters in land–atmosphere interactions. LST controls the upward terrestrial radiation and surface-atmosphere sensible and latent heat fluxes, and it is an indicator of the energy balance at the earth's surface (Sellers et al., 1997; Sun and Pinker, 2003; Pinker et al., 2009).

In this study, a distributed biosphere hydrological model, the so-called water and energy budget-based distributed hydrological model (WEB-DHM; Wang et al., 2009; Wang and Koike, 2009), is evaluated against observed streamflows and MODIS LSTs. The model is then used to investigate the water and energy cycles of the upper Tone River Basin.

Distributed biosphere hydrological model

The distributed biosphere hydrological model, WEB-DHM (Wang et al., 2009; Wang and Koike, 2009) was developed by fully coupling a biosphere scheme (SiB2; Sellers et al., 1996a) with a geomorphology-based hydrological model (GBHM; Yang, 1998). The model enabled consistent descriptions of water, energy and CO_2 fluxes at a basin scale.

The characteristics of the WEB-DHM are summarized as follows. First, the model physically describes ET using a biophysical land surface scheme (SiB2; Sellers et al., 1996a) for simultaneously simulating heat, moisture, and CO_2 fluxes in the soil–vegetation–atmosphere transfer (SVAT) processes. Second, the hydrological submodel describes overland, lateral subsurface, and groundwater flows using grid-hillslope discretization and then flow routing in the river network. Third, the model has high efficiency for simulations of large-scale river basins while incorporating subgrid topography. This is because the WEB-DHM, which inherits the spatial structure of GBHM, employs catchment and width functions to combine the topography (see Yang et al., 2000) and integrates the hillslopes within one large model grid using a subgrid parameterization (Wang et al., 2009).

Model structure

The overall model structure is shown in Fig. 2 and can be described as follows:

(1) A digital elevation model (DEM) is used to define the target area. The target basin is then divided into sub-basins according to the DEM resolution and the needs of the model simulation (see Fig. 2a).
(2) Within a given sub-basin, a number of flow intervals are specified to represent time lags and the accumulating processes in the river network according to the distance to the outlet of the sub-basin. Each flow interval includes several model grids (see Fig. 2b).
(3) For each model grid with one combination of land use type and soil type, the SiB2 is used to independently calculate turbulent fluxes between the atmosphere and land surface (see Fig. 2b and d). The vertical distributions of water for all the model grids in the target basin, such as ground interception storage and soil moisture within the soil profile, can be obtained through this biophysical process.
(4) Each model grid is subdivided into a number of geometrically symmetrical hillslopes (see Fig. 2c). A hillslope with unit length is called a basic hydrological unit (BHU) of the WEB-DHM. For each BHU, the hydrological submodel is used to simulate lateral water redistributions and calculate runoff comprised of overland, lateral subsurface and groundwater flows (see Fig. 2c and d). The runoff for a model grid is the total response of all BHUs within it.
(5) The length of a flow interval is usually assigned as 1.5 or 2 times the model grid size. In practice it is difficult to identify and represent all the river channels in a grid-based DHM. For simplicity, the streams located in one flow interval are combined into a single virtual channel. All the flow intervals are linked by the river network generated from the DEM. All runoff from the model grids in the given flow interval is accumulated into the virtual channel and led to the outlet of the river basin.

Simplifications have been made to reduce computation costs. First, interactions of groundwater between flow intervals are not considered. Second, within a flow interval, the lateral moisture exchanges between model grids are not formulated. Third, all streams ($\sum L$) extracted from the fine DEM within a given model grid (Fig. 2c) can be simplified as one stream with the same length ($\sum L$) flowing along the main flow direction of the model grid. Therefore, the total runoff generated from a given model grid can be regarded as being from the new hillslopes along the single stream.

Subgrid parameterization

When a fine DEM is available and simulation is performed in larger model grids, a subgrid parameterization scheme is used to capture topographical characteristics. Each BHU (hillslope) is actually a conceptual element in a large model grid (Fig. 2c). The hillslope parameters (length and slope) for each model grid are obtained by preprocessing of the fine DEM.

Please cite this article in press as: Wang, L., et al. Assessment of a distributed biosphere hydrological model against streamflow and MODIS land surface temperature in the upper Tone River Basin. J. Hydrol. (2009), doi:10.1016/j.jhydrol.2009.08.005

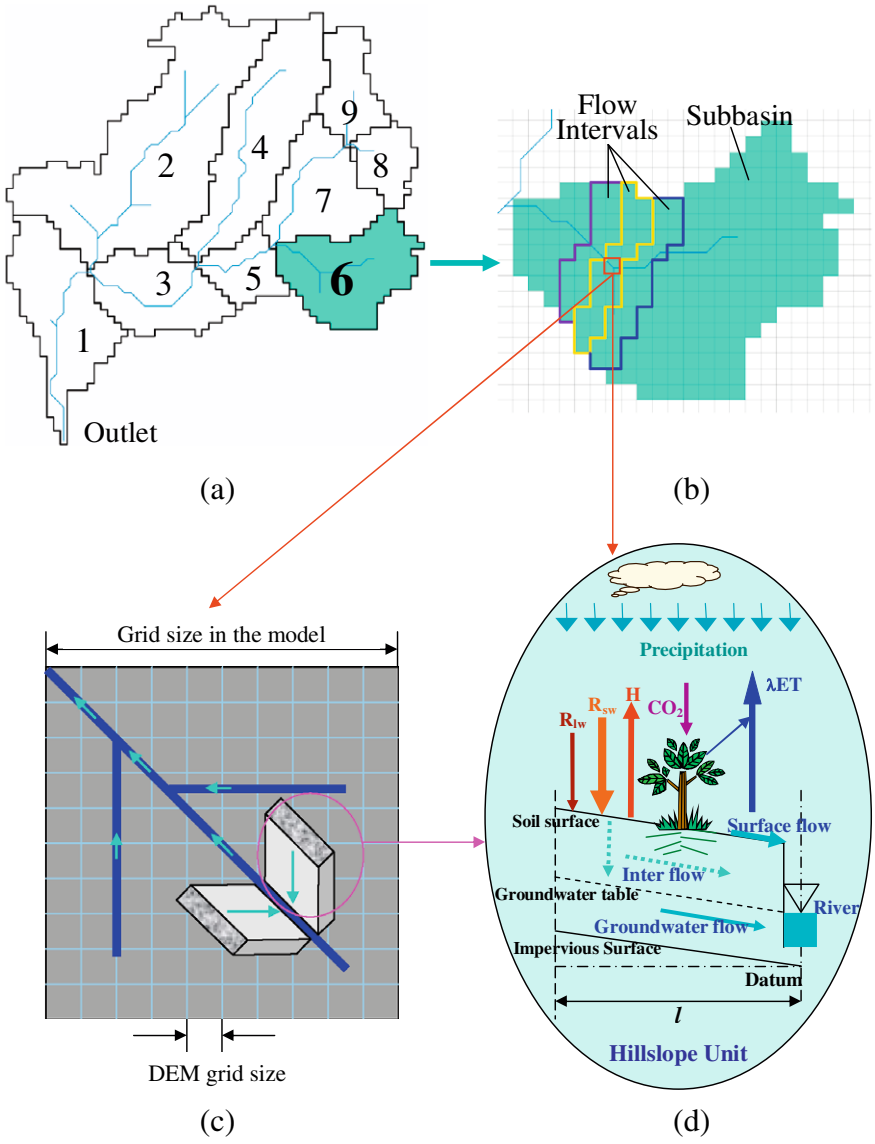

Fig. 2. Overall structure of WEB-DHM: (a) division from basin to sub-basins, (b) subdivision from sub-basin to flow intervals comprising several WEB-DHM grids, (c) discretization from a WEB-DHM grid to a number of geometrically symmetrical hillslopes, and (d) description of the water moisture transfer from atmosphere to river. Here, SiB2 is used to describe the transfer of the turbulent fluxes (energy, water, and CO_2) between atmosphere and ground surface for each WEB-DHM grid, where R_{sw} and R_{lw} are downward solar radiation and longwave radiation, respectively, H is the sensible heat flux, and λ is the latent heat of vaporization; GBHM simulates both surface and subsurface runoff using grid-hillslope discretization, and then simulates flow routing in the river network.

As illustrated in Fig. 2c, it is assumed that a large model grid comprises a set of symmetrical hillslopes located along the streams. Within a model grid, all hillslopes are viewed as being geometrically similar. A hillslope with unit width is a BHU and is represented by a rectangular inclined plane. The hillslope length within a model grid is calculated as

$$l = A \Big/ 2 \sum L, \tag{1}$$

where A is the model grid area and $\sum L$ is the total length of streams within the model grid extracted from the fine DEM. The total river length $\sum L$ decreases with increasing threshold area (O'Callaghan and Mark, 1984; Tarboton et al., 1991). The model grid slope is taken to be the mean of all subgrid slopes in the fine DEM.

Land surface temperature

The land surface submodel (SiB2) simulates energy and mass transfers among the soil, vegetation, and the atmosphere. Details about the formulations of SiB2 are in Sellers et al. (1996a). The hydrological submodel describing lateral flows and river routing can be found in Wang et al. (2009). Here, the governing equations for land surface temperature are described in details.

The land surface submodel has 11 prognostic physical state variables: temperatures for canopy (T_c), soil surface (T_g), and deep soil (T_d); interception water stores for canopy (M_{cw}), and soil surface (M_{gw}); interception snow/ice stores for canopy (M_{cs}) and soil surface (M_{gs}); soil wetness in the first layer (W_1), root zone (W_2) and deep soil zone (W_3); and canopy conductance (g_c). The governing equations for temperatures are given as follows (Sellers et al., 1996a).

$$\text{Canopy} \quad C_c \frac{\partial T_c}{\partial t} = Rn_c - H_c - \lambda E_c - \xi_{cs}, \tag{2}$$

$$\text{Soil surface} \quad C_g \frac{\partial T_g}{\partial t} = Rn_g - H_g - \lambda E_g - \frac{2\pi C_d}{\tau_d}(T_g - T_d) - \xi_{gs}, \tag{3}$$

Please cite this article in press as: Wang, L., et al. Assessment of a distributed biosphere hydrological model against streamflow and MODIS land surface temperature in the upper Tone River Basin. J. Hydrol. (2009), doi:10.1016/j.jhydrol.2009.08.005

$$\text{Deep soil} \quad C_d \frac{\partial T_d}{\partial t} = \frac{1}{2(365\pi)^{1/2}}(Rn_g - H_g - \lambda E_g), \tag{4}$$

where Rn_c, Rn_g are absorbed net radiations (W m^{-2}); H_c, H_g are sensible heat fluxes (W m^{-2}); E_c, E_g are evapotranspiration rates (kg m^{-2} s^{-1}); C_c, C_g, C_d are effective heat capacities (J m^{-2} K^{-1}); λ is latent heat of vaporization (J kg^{-1}); τ_d is daylength (s); and ξ_{cs}, ξ_{gs} are energy transfers due to phase changes in M_c ($=M_{cw}+M_{cs}$) and M_g ($=M_{gw}+M_{gs}$), respectively (W m^{-2}). The subscript "c" refers to the canopy, "g" to the soil surface, and "d" to the deep soil. The equations for calculating C_c, C_g, C_d are in Appendix E of Sellers et al. (1996a).

In the MODIS LST product, LST is the radiometric (kinetic) temperature related to the thermal infrared (TIR) radiation emitted from the land surface observed by an instantaneous MODIS observation (Wan, 2008), where land surface means the top of the canopy in vegetated areas or the soil surface in bare areas. For a model grid of mixed vegetation and bare soil, the LST can be estimated from T_c and T_g if the emissivity of the model grid is assumed as homogeneous (Becker and Li, 1995; Norman and Becker, 1995)

$$T_{sim} = \left[VT_c^4 + (1-V)T_g^4\right]^{1/4} \tag{5}$$

where V is green vegetation coverage assumed it varies temporally in the study, which can be describe as (Kerr et al., 1992)

$$V = (NDVI - NDVI_{\min})/(NDVI_{\max} - NDVI_{\min}). \tag{6}$$

On the other hand, the LAI has the relationship with $NDVI$ as (Yin and Williams, 1997)

$$LAI = LAI_{\max} * (NDVI - NDVI_{\min})/(NDVI_{\max} - NDVI_{\min}). \tag{7}$$

Therefore, the green vegetation coverage V can be derived as

$$V = LAI/LAI_{\max}, \tag{8}$$

where the maximum LAI values ($LAI_{\max}$) can be derived following Sellers et al. (1996b).

Datasets

The datasets of the upper Tone River Basin, as used in WEB-DHM, are as described below.

Digital data of elevation, and land use were obtained from the Japan Geographical Survey Institute. Subgrid topography was described by a 50 m resolution DEM. The elevation of this basin varies from about 100 m to 2500 m (upper left, Fig. 3). Grid slopes vary from 0° to 39° with a mean value of 16° for model grids (see Fig. 3, upper right). Land use data was reclassified to 3 SiB2 categories, with broadleaf-deciduous trees as the dominant type (more than 85%) (Fig. 3, lower left). The vegetation static parameters including morphological, optical and physiological properties were defined following Sellers et al. (1996b). The dynamic vegetation parameters are Leaf Area Index (LAI), and the Fraction of Photosynthetically Active Radiation (FPAR) absorbed by the green vegetation canopy, and can be obtained from satellite data. Global LAI and FPAR MOD15_BU 1 km data sets (Myneni et al., 1997) were used in this study. These are 8-daily composites of MOD15A2 products and are from the EOS Data Gateway of NASA. The MODIS LST V5 products (Wan, 2008) used in this paper were also from the EOS Data Gateway of NASA. These are also 1-km 8-daily composites

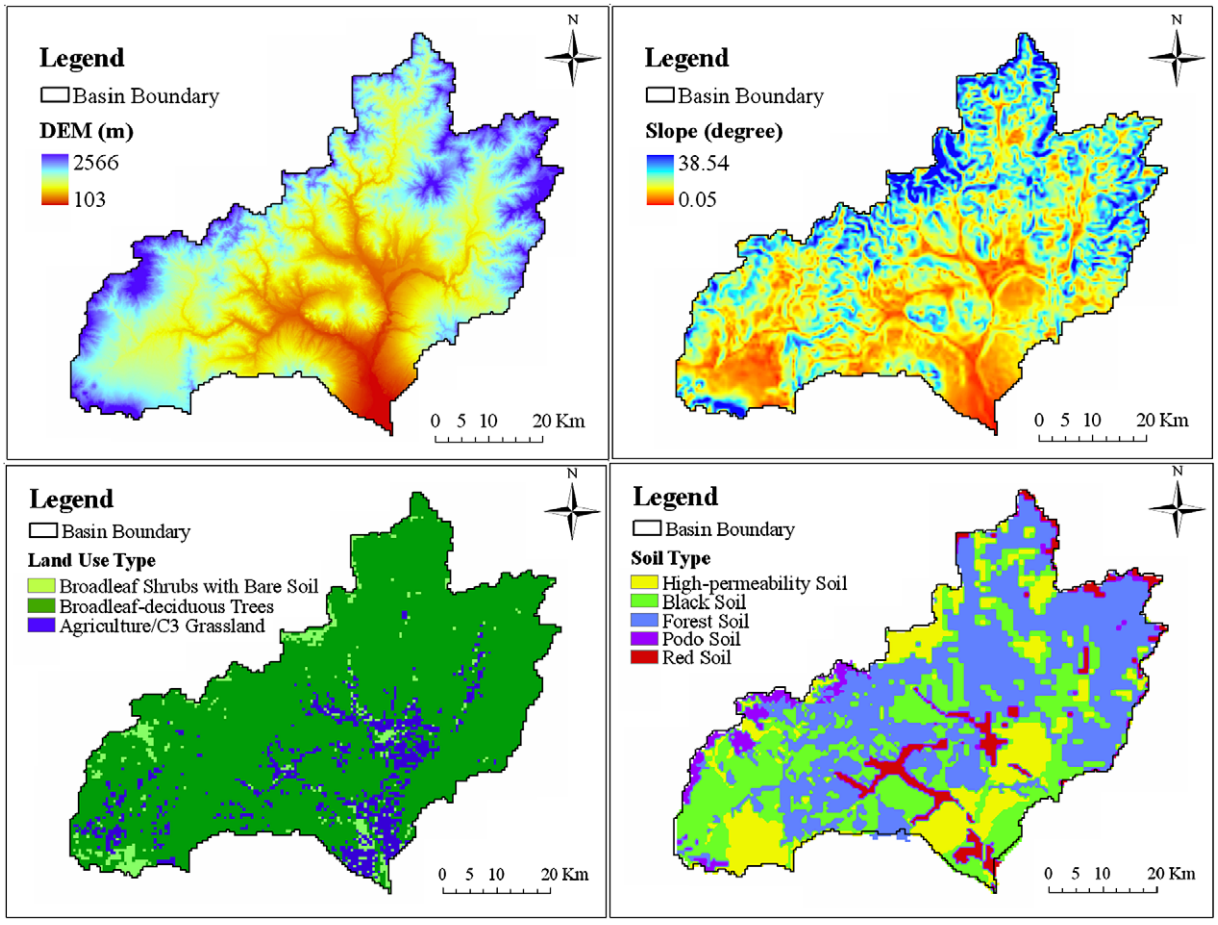

Fig. 3. Spatial distribution of DEM, grid slope, land use, and soil type in the upper Tone River Basin.

Please cite this article in press as: Wang, L., et al. Assessment of a distributed biosphere hydrological model against streamflow and MODIS land surface temperature in the upper Tone River Basin. J. Hydrol. (2009), doi:10.1016/j.jhydrol.2009.08.005

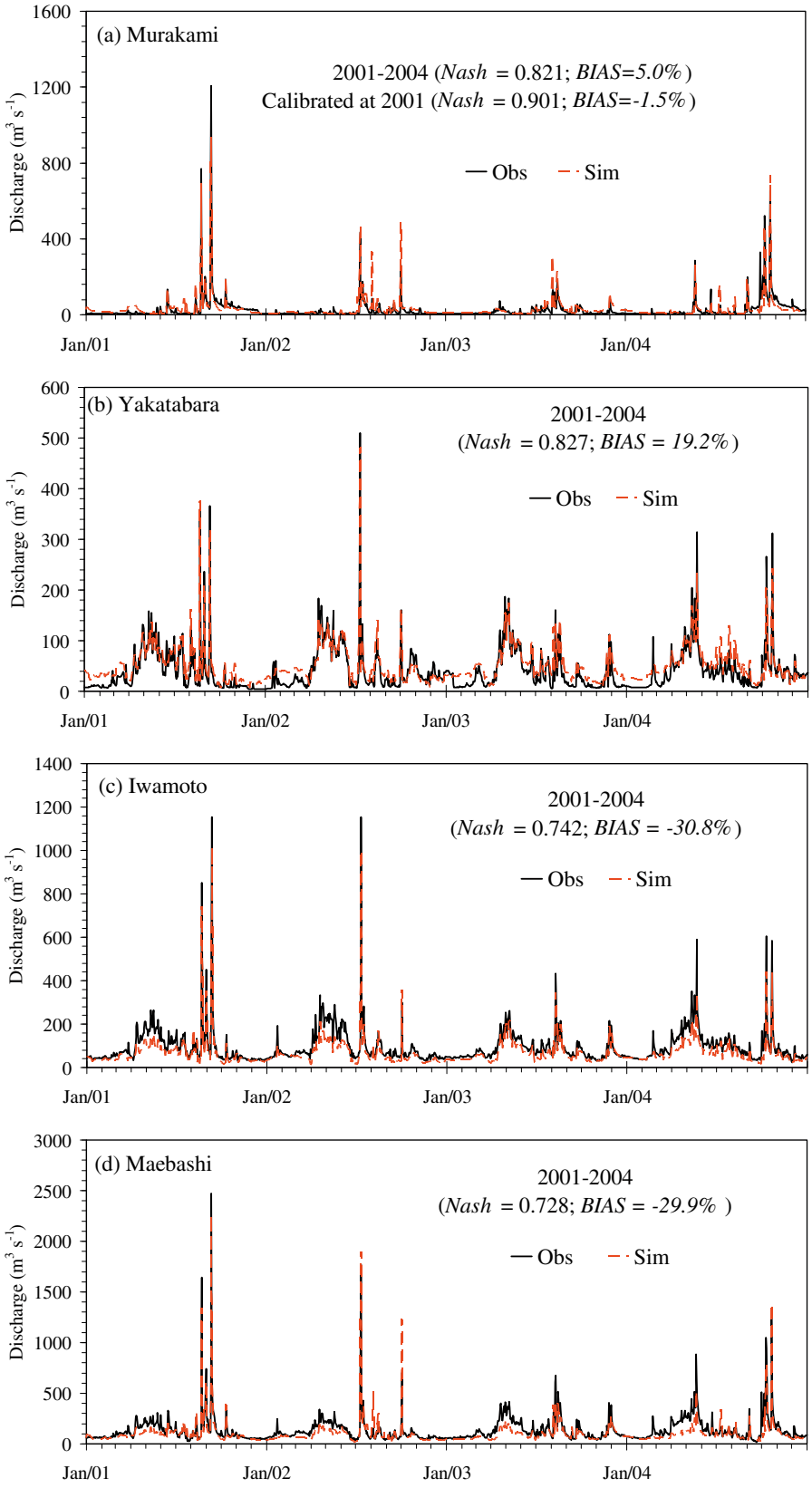

Fig. 4. Observed and simulated daily streamflows at four control stations (Murakami (a), Yakatabara (b), Iwamoto (c), and Maebashi (d)) in the upper Tone River Basin from 2001 to 2004. The model was only optimized at Murakami, using 2001 data.

having cloud-contaminated LST values removed. The soil map (Fig. 3, lower right) is processed from a 1:200,000 scale Gunma Prefecture geological map.

Hourly precipitation data were obtained from Radar-AMeDAS (Automated Meteorological Data Acquisition System) rainfall analysis data, which combines both radar and ground observations, and

Please cite this article in press as: Wang, L., et al. Assessment of a distributed biosphere hydrological model against streamflow and MODIS land surface temperature in the upper Tone River Basin. J. Hydrol. (2009), doi:10.1016/j.jhydrol.2009.08.005

was provided by the Japanese Meteorological Agency (JMA). The data were available at 5 km spatial resolution until March of 2001 and at 2.5 km spatial resolution after that. Surface meteorological data other than precipitation, comprise air temperature, relative humidity, air pressure, and wind speed, as well as downward solar and longwave radiation. In this basin, the observed air temperature, wind speed, and sunshine duration were available from 15 meteorological sites (see Fig. 1) in hourly resolution from the

Table 1
Basin-averaged values of the parameters used in the upper Tone River Basin.

Symbol	Parameters	Unit	Basin-averaged value	Source
θ_s	Saturated water content		0.51	FAO (2003)
θ_r	Residual water content		0.17	FAO (2003)
α	van Genuchten parameter		0.01746	FAO (2003)
n	van Genuchten parameter		1.524	FAO (2003)
anik	Hydraulic conductivity anisotropy ratio		15.6	Optimization
f	Hydraulic conductivity decay factor		0.5	Optimization
Mgw_{max}	Maximum surface water detention	m	0.01	Optimization
K_s	Saturated hydraulic conductivity for soil surface	mm h^{-1}	104.0	Optimization
K_g	Hydraulic conductivity of groundwater	mm h^{-1}	1.0	Yang et al. (2004)
D_r	Root depth ($D_1 + D_2$)	m	1.43	Sellers et al. (1996b)

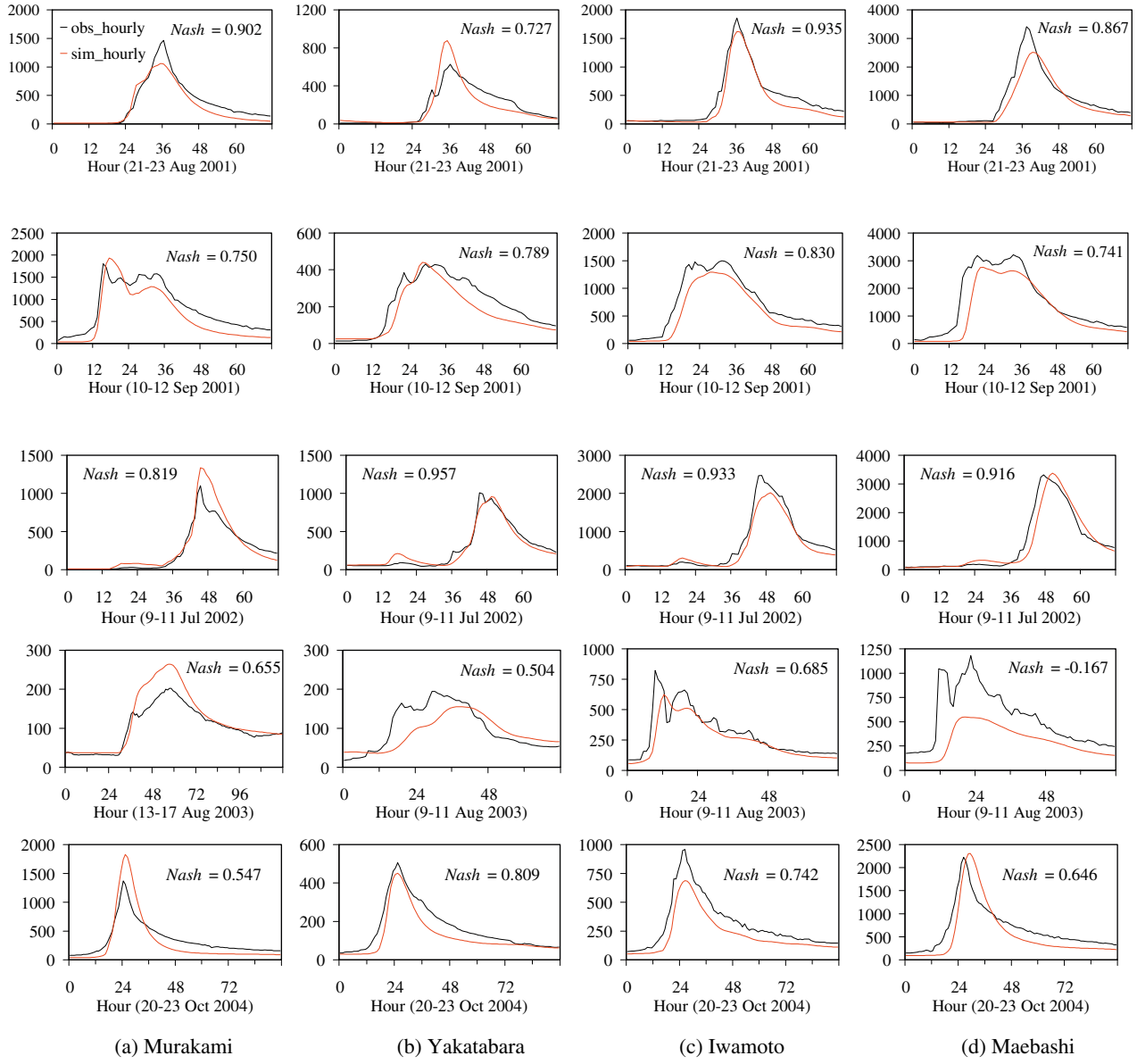

Fig. 5. Observed and simulated hourly annual largest flood peaks at the stream gauges of Murakami (a), Yakatabara (b), Iwamoto (c), and Maebashi (d) from 2001 to 2004, with Nash–Sutcliffe coefficient (*Nash*). The *y* axis represents discharge ($m^3\ s^{-1}$).

Please cite this article in press as: Wang, L., et al. Assessment of a distributed biosphere hydrological model against streamflow and MODIS land surface temperature in the upper Tone River Basin. J. Hydrol. (2009), doi:10.1016/j.jhydrol.2009.08.005

Table 2
Comparison of observed and simulated annual largest flood peaks occurring at the main discharge gauges in the upper Tone River Basin (flood peak: $m^3 s^{-1}$, time: date (h)).

Year	Gauge	Observed (*Obs*)		Simulated (*Sim*)		Difference (*Dif*)		*Dif*/*Obs*
		Flood	Time	Flood	Time	Flood	Time (h)	Flood (%)
2001(1)	Murakami	1467	Aug22(13)	1058	Aug22(12)	−409	−1	−28
	Yakatabara	627	Aug22(13)	876	Aug22(12)	249	−1	40
	Iwamoto	1856	Aug22(13)	1620	Aug22(13)	−236	0	−13
	Maebashi	3407	Aug22(14)	2515	Aug22(16)	−892	2	−26
2001(2)	Murakami	1802	Sep10(16)	1933	Sep10(18)	131	2	7
	Yakatabara	431	Sep11(06)	441	Sep11(05)	10	−1	2
	Iwamoto	1496	Sep11(08)	1289	Sep11(04)	−207	4	−14
	Maebashi	3208	Sep11(10)	2762	Sep10(24)	−446	10	−14
2002	Murakami	1103	Jul10(22)	1334	Jul10(22)	231	0	21
	Yakatabara	1008	Jul10(22)	955	Jul11(02)	−53	4	−5
	Iwamoto	2473	Jul10(23)	2020	Jul11(02)	−453	3	−18
	Maebashi	3319	Jul10(24)	3380	Jul11(03)	61	3	2
2003	Murakami	202	Aug15(11)	264	Aug15(11)	62	0	31
	Yakatabara	195	Aug10(07)	155	Aug10(15)	−40	8	−21
	Iwamoto	822	Aug09(10)	624	Aug09(13)	−198	3	−24
	Maebashi	1178	Aug09(23)	549	Aug09(21)	−629	−2	−53
2004	Murakami	1368	Oct21(01)	1827	Oct21(02)	459	1	34
	Yakatabara	506	Oct21(02)	450	Oct21(02)	−56	0	−11
	Iwamoto	957	Oct21(03)	686	Oct21(03)	−271	0	−28
	Maebashi	2224	Oct21(03)	2309	Oct21(06)	85	3	4

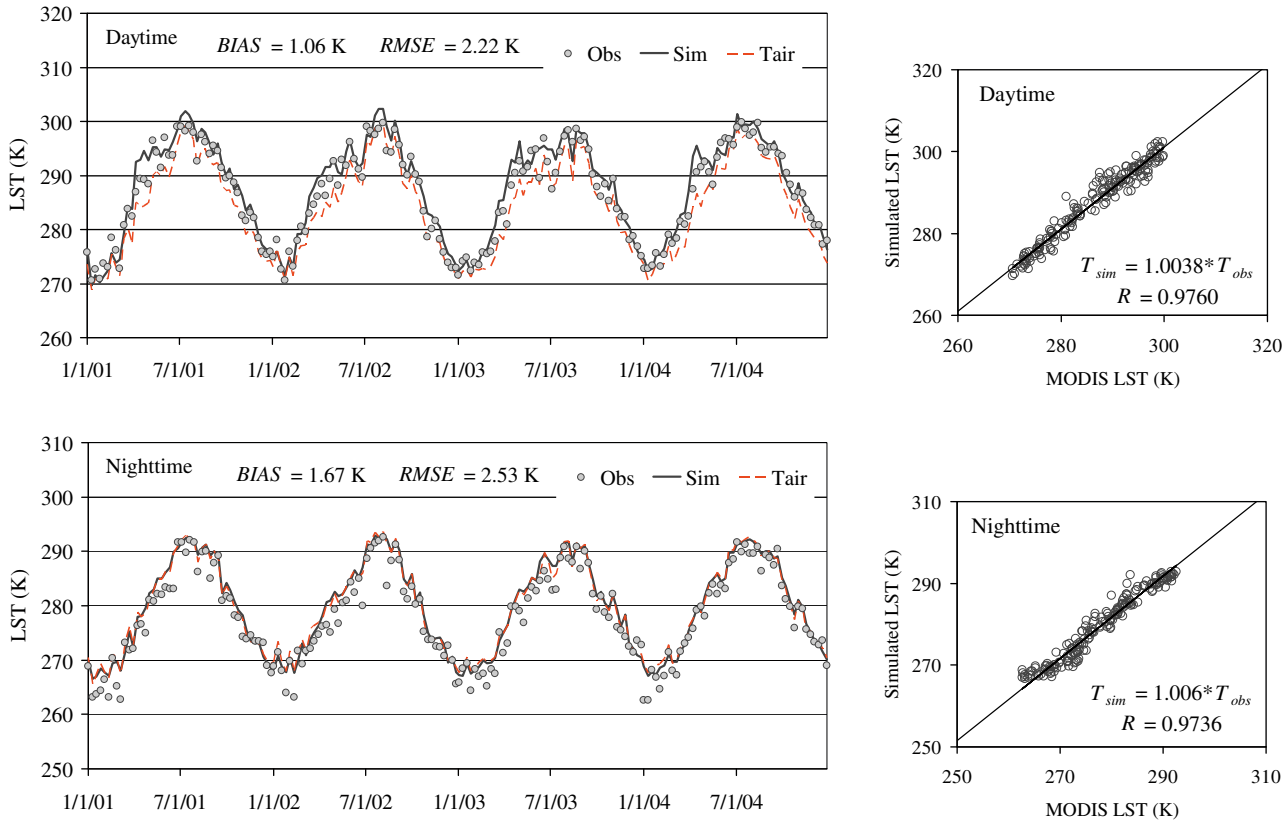

Fig. 6. Comparison of 8-daily LSTs between model simulations (T_{sim}) and MODIS observations (T_{obs}) during daytime (upper) and nighttime (lower) averaged for the upper Tone River Basin from 2001 to 2004. Time-series (left) and scatter plots (right). Here, the missing data in MODIS LSTs and their corresponding simulated LSTs, and input air temperature have been exempted for comparison.

AMeDAS annual report of the JMA. Relative humidity and air pressure were obtained from three radiation stations maintained by JMA and interpolated into the 15 meteorological sites using the Angular distance-weighted (ADW) interpolation method (New et al., 2000). Downward solar radiation was then estimated from sunshine duration, temperature, and humidity, using a hybrid model developed by Yang et al. (2001, 2006). This model can effectively account for the effect of elevation and humidity on radiative transfer processes, and has been well validated in lowland/highland and humid/dry regions. Longwave radiation was then estimated from temperature, relative humidity, pressure, and solar radiation using the relationship between solar radiation and longwave radiation (Crawford and Duchon, 1999).

Precipitation data were linearly interpolated from coarser (5 km or 2.5 km) grids to model (500 m) grids, while all the other meteorological variables (including wind speed) were interpolated to

Please cite this article in press as: Wang, L., et al. Assessment of a distributed biosphere hydrological model against streamflow and MODIS land surface temperature in the upper Tone River Basin. J. Hydrol. (2009), doi:10.1016/j.jhydrol.2009.08.005

500 m grids for model simulations using the ADW interpolation method (New et al., 2000). The interpolated surface air temperature inputs are further modified with a lapse rate of 6.5 K km^{-1}, considering the elevation differences between the model grids and meteorological stations. However, the altitudinal effect on relative humidity is assumed negligible.

Model evaluation

The aim of this study was to investigate the water and energy cycles of the upper Tone River Basin with WEB-DHM and MODIS LST products. First, the model was calibrated and validated for discharges at four major stream gauges (Fig. 1). Second, the model was again verified using the MODIS LSTs in both basin-averaged values and spatial patterns. Finally, the basin- and sub-basin-scale water and energy cycles were analyzed and discussed.

For simplification, the water bodies (several reservoirs) in upper mountainous regions were not considered in the simulations of land–atmosphere interactions because of their small areas (less than 1.5% of the upper Tone River Basin).

Evaluation with discharges

Four-year (2001–2004) meteorological data with 500 m grid size and hourly time step, was prepared for the study region. The initial conditions were obtained by running the model several times with forcing data from 2001 to 2004 until a hydrological equilibrium was reached. The model was calibrated using the data of year 2001 at the Murakami gauge and validated with other years from this gauge. Further validations were carried out at the other three discharge gauges (Yakatabara, Iwamoto, and Maebashi) from 2001 to 2004. As shown in Fig. 1, the releases from three reservoirs (Aimata, Fujiwara, and Sonohara) were used in the simulations as the discharges from their upper regions. Obviously, the outflows from Aimata and Fujiwara reservoirs contribute to the observed discharges of Yakatabara; while Iwamoto and Maebashi are affected by all three reservoirs. The Murakami is disturbed by none of them and thus was used to calibrate parameters.

Fig. 4a shows the calibrated daily hydrograph at the Murakami gauge with Nash–Sutcliffe model efficiency coefficient (*Nash*) (Nash and Sutcliffe, 1970). Where, *Nash* is defined as

$$Nash = 1 - \sum_{i=1}^{n}(Q_{oi} - Q_{si})^2 \Big/ \sum_{i=1}^{n}(Q_{oi} - \overline{Q_o})^2, \quad (9)$$

where Q_{oi} is observed discharge; Q_{si} is simulated discharge; n is the total number of time-series for comparison; and $\overline{Q_o}$ is the mean value of the discharge observed over the simulation period. The higher *Nash* is, the better the model performs. A perfect fit should have a *Nash* value equal to one. The van Genuchten parameters (α and n), saturated water content (θ_s), and residual water content (θ_r) were obtained from FAO (2003). The saturated hydraulic conductivity for soil surface (K_s), the hydraulic conductivity anisotropy ratio (*anik*), and the hydraulic conductivity decay factor (f), as well as the maximum surface water detention (Mgw_{max}) were calibrated by matching simulated and observed discharges. Optimized values of the spatial averages of the parameters are listed in Table 1, where K_s decreases from high-permeability soil to black soil, with optimized values of 170 mm h^{-1} for high-permeability soil, 53 mm h^{-1} for black soil, and 107 mm h^{-1} for forest soil, as well as 128 mm h^{-1} for podo and red soils.

After the calibration, the model reproduces the discharge of Murakami very well with *Nash* equal to 0.901 and the bias error (*BIAS*) −1.5% for 2001 (Fig. 4a). By keeping theses parameters constant, the model was used for the validation at four major control gauges (Murakami, Yakatabara, Iwamoto, and Maebashi) in the basin from 2001 to 2004. Fig. 4 shows the daily hydrographs from 2001 to 2004 for the four stream gauges. At Murakami with little dam effect, the simulated discharges also show good agreements with observed ones with the *Nash* equal to 0.821 and the *BIAS* 5.0% (Fig. 4a). The daily hydrographs at the other three stream gauges (Yakatabara, Iwamoto, and Maebashi), given in Fig. 4b–d, also give acceptable accuracies with *Nash* equal to 0.827, 0.742, and 0.728 and the *BIAS* equal to 19.2%, −30.8%, and −29.9%, respectively.

The simulated hourly annual largest flood peaks during the long-term continuous simulation from 2001 to 2004 are compared with hourly ground observations in Fig. 5 and Table 2. In 2001, there were two continuous large flood peaks with the former occurring 21–23 August and the latter 10–12 September. Generally, in the long-term continuous simulations, hourly annual largest flood peaks at the four control stations are well reproduced with most *Nash* greater than 0.7 (see Fig. 5). In most cases, the differences between simulated and observed annual largest flood peaks are less than 25% (Table 2). The flood peak time are well reproduced with almost all the time differences less than 4 h (see Table 2).

Evaluation with MODIS LST

For energy balances in the basin, it was impossible to show comparisons between simulated and observed energy budget components because of a lack of flux observations.

Fortunately, the recently-released MODIS LST V5 products (Wan, 2008) with global coverage and high resolution (the finest is 1 km grid), provided us unique tools to improve our basin-scale energy budget study. Because LST is a crucial parameter in the physics of land surface processes at regional and global scales, combining, as it does, the results of all surface-atmosphere interactions and energy fluxes between the atmosphere and the ground. New refinements for V5 products significantly improved the spa-

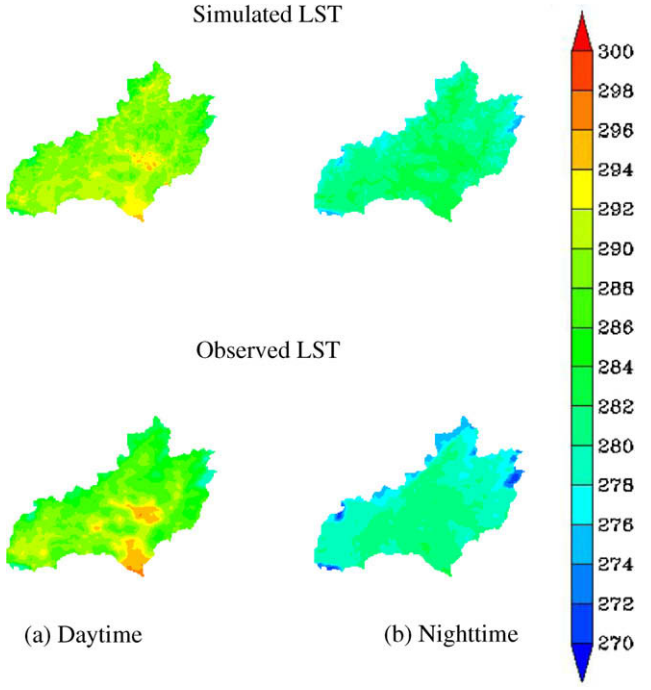

Fig. 7. Spatial distribution of mean LSTs (2001–2004) (unit: K) during daytime (a) and nighttime (b) by model simulations (upper) compared to MODIS observations (lower) in the upper Tone River Basin. Here, the missing data in MODIS LSTs and their corresponding simulated LSTs have been exempted for comparison.

Please cite this article in press as: Wang, L., et al. Assessment of a distributed biosphere hydrological model against streamflow and MODIS land surface temperature in the upper Tone River Basin. J. Hydrol. (2009), doi:10.1016/j.jhydrol.2009.08.005

tial coverage of LSTs, especially in highland regions, and increased the accuracy and stability of MODIS LST products. Comparisons between V5 LSTs and in situ values in 47 clear-sky cases (LST range from −10 °C to 58 °C, and atmospheric column water vapor range from 0.4 to 3.5 cm) indicate that the accuracy of the MODIS LST products is better than 1 K in most cases (39 out of 47) and the root mean squared error (*RMSE*) is less than 0.7 K for all 47 cases (Wan, 2008).

Since the WEB-DHM has been validated by simulating multiple-site streamflows in the upper Tone River Basin, once the model has been again verified with basin-scale evolution of MODIS LSTs, greater confidence can be obtained for further analyses on water and energy cycles in the basin. Here, the missing data in 8-daily MODIS LSTs and their corresponding simulated LSTs have been exempted for comparison.

Fig. 6 shows a comparison of 8-daily LSTs between the model simulation (T_{sim}) and MODIS products (T_{obs}) at daytime (around 10:30, local time) and nighttime (around 22:30, local time) averaged for the upper Tone River Basin from 2001 to 2004. Results show that the simulated daytime LSTs agree well with MODIS LSTs with the *BIAS* equal to 1.06 K and the *RMSE* equal to 2.22 K; while the nighttime LSTs are slightly overestimated by the model with the *BIAS* equal to 1.67 K and the *RMSE* equal to 2.53 K. The *BIAS* and *RMSE* of the input air temperature (T_{air}) field with respect to MODIS LSTs at daytime are −2.42 K and 2.90 K, respectively; while at nighttime 1.68 K and 2.42 K, respectively. At daytime, the *BIAS* and *RMSE* reduction for the modeled LSTs with respect to the T_{air} is a relevant indication that the model properly represent the surface energy balance. At nighttime, both the simulated LSTs and MODIS LSTs appear very close to the nighttime T_{air}. It is not surprising since at the nighttime the land surface is mainly heated by the downward longwave raidation from the air space. The scatterplots are also given for both daytime and nighttime LSTs, which confirm the general good performance by WEB-DHM in simulating basin-averaged LSTs.

Fig. 7 gives the spatial distribution of mean LSTs in daytime and nighttime by model simulation compared to MODIS observations in the upper Tone River Basin from 2001 to 2004. In general, the patterns of simulated LSTs in daytime and nighttime appear very similar to the MODIS LSTs, except for some differences in small regions. The underestimates of the daytime LSTs by the model occur in the center and the lower parts of the basin (Fig. 7), where are urbanized areas but are classified as agriculture/C3 grassland or

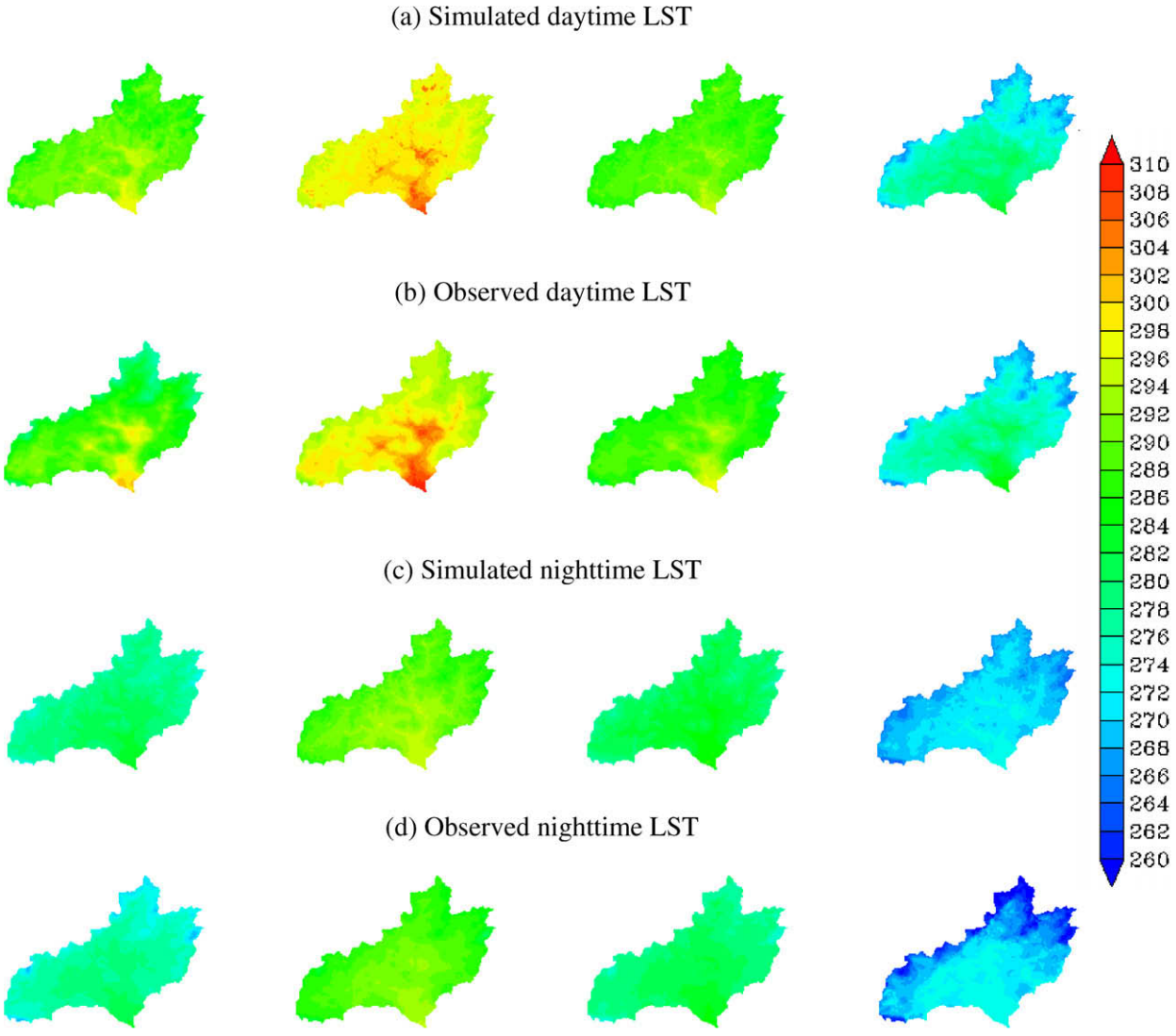

Fig. 8. Seasonal changes (MAM, JJA, SON, and DJF are listed from left to right) of the spatial distribution for daytime and nighttime LSTs (unit: K) by model simulations (a and c) compared to MODIS observations (b and d) in the upper Tone River Basin from 2001 to 2004. Here, the missing data in MODIS LSTs and their corresponding simulated LSTs have been exempted for comparison.

Please cite this article in press as: Wang, L., et al. Assessment of a distributed biosphere hydrological model against streamflow and MODIS land surface temperature in the upper Tone River Basin. J. Hydrol. (2009), doi:10.1016/j.jhydrol.2009.08.005

broadleaf shrubs with bare soil in SiB2 land use map (see Fig. 3). The overestimates of the modeled daytime and nighttime LSTs in the area with highest altitudes are possibly attributed to the errors in input air temperature. Due to no meteorological sites available, a homogeneous lapse rate (6.5 K km^{-1}) has been adopted to account for the air temperature dependence on elevation, and therefore, errors in the interpolated air temperature may occur in the uppermost mountain regions.

Fig. 8 displays the seasonal changes of the spatial distribution of daytime and nighttime LSTs by model simulation compared to MODIS observations. The patterns of simulated LSTs in different seasons are again visually similar to the MODIS LSTs, but the model simulation underestimates the daytime LSTs for the central and lower regions (especially for the daytime LSTs in MAM and JJA), and overestimates both the daytime and nighttime LSTs for the uppermost mountain regions (especially for the daytime LSTs in JJA, and for the nighttime LSTs in DFJ).

Analyses on the basin- and sub-basin-scale water and energy cycles

After evaluations with observed streamflows and LSTs, the model demonstrated its good performance in representing both water and energy processes. Next step, the model is used to investigate basin- and sub-basin-scale water and energy cycles.

Fig. 9 plots the 4-year (2001–2004) averaged net radiation, ground heat flux, sensible heat flux, latent heat flux, deep soil wetness and water table depth simulated by WEB-DHM. The mean simulated sensible heat flux is relatively small, and is determined by the temperature difference between the land surface and air. The mean simulated latent heat flux (LE) gives an obvious zonal distribution with an increasing trend from the upper mountainous areas to the lower plains; generally being controlled by the absorbed net radiation by the land surface and the available soil moisture, as well as other land surface meteorology (e.g., precipita-

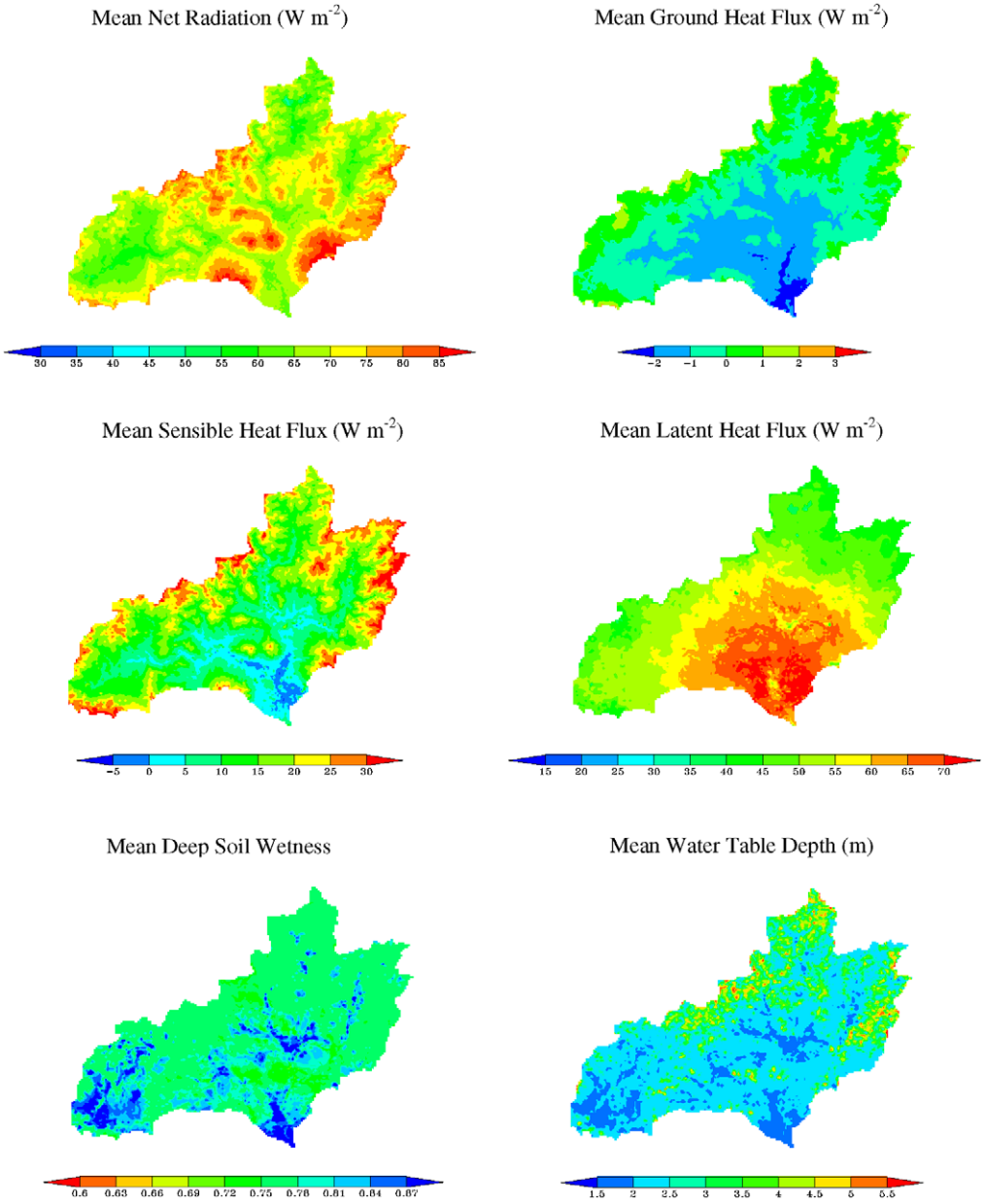

Fig. 9. Plots of 4-year (2001–2004) averaged net radiation, ground heat flux, sensible heat flux, latent heat flux, deep soil wetness, and water table depth simulated by WEB-DHM.

Please cite this article in press as: Wang, L., et al. Assessment of a distributed biosphere hydrological model against streamflow and MODIS land surface temperature in the upper Tone River Basin. J. Hydrol. (2009), doi:10.1016/j.jhydrol.2009.08.005

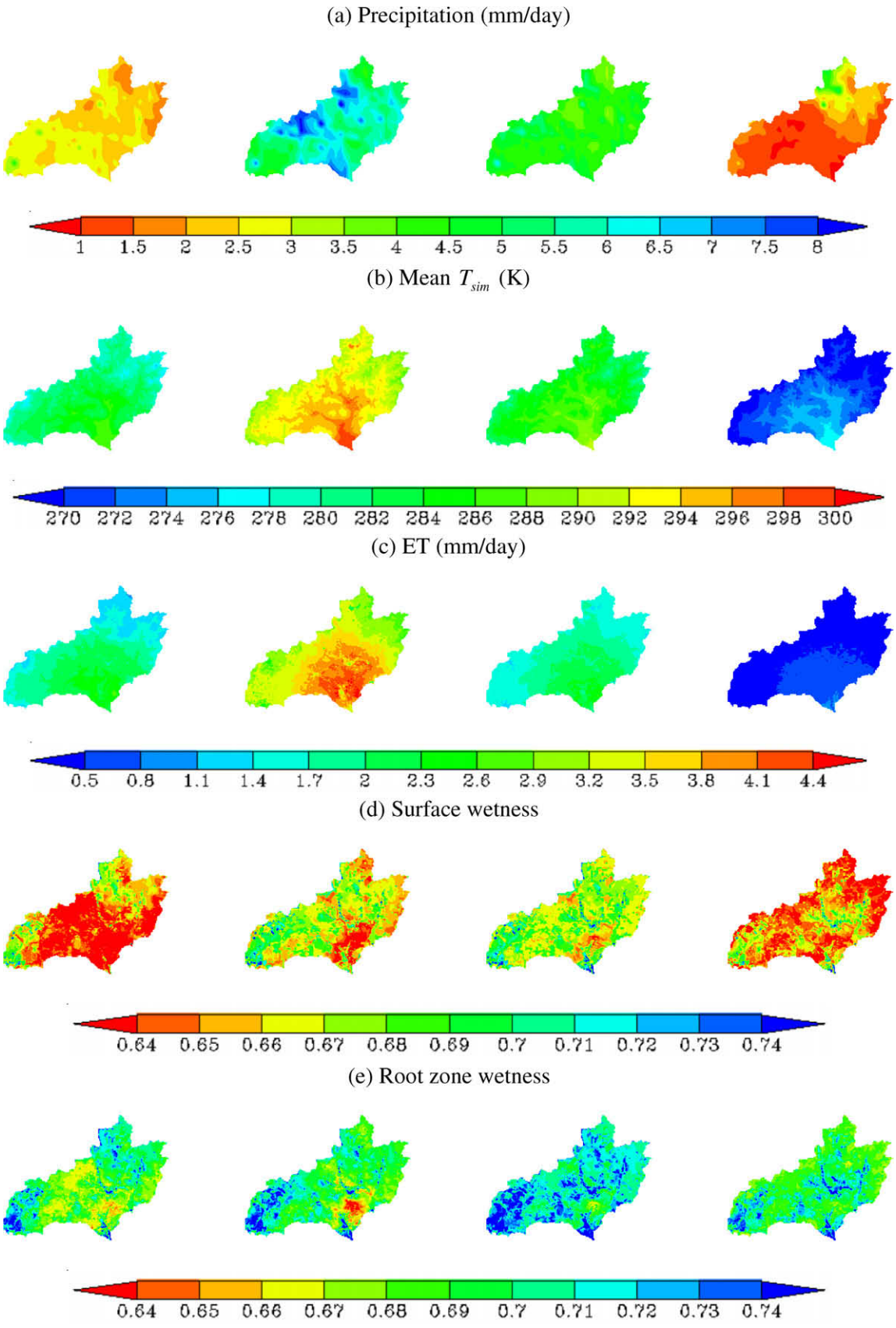

Fig. 10. Seasonal changes (MAM, JJA, SON, and DJF are listed from left to right) of the spatial distributions of precipitation (a), simulated mean LST (b), ET (c), surface wetness (d), and root zone wetness (e) in the upper Tone River Basin from 2001 to 2004.

tion, air humidity, wind speed) and vegetation conditions. The mean simulated net radiation and ground heat flux are included to close the surface energy budget. The pattern of the simulated mean deep soil wetness is consistent with the water table depth,

Please cite this article in press as: Wang, L., et al. Assessment of a distributed biosphere hydrological model against streamflow and MODIS land surface temperature in the upper Tone River Basin. J. Hydrol. (2009), doi:10.1016/j.jhydrol.2009.08.005

having wetter soil in areas with lower water tables, while the water table depth closely follows the grid slope in the model (Figs. 3 and 9). The water table exhibits a spatial structure that is influenced by the grid slope and is characterized by relatively shallow water levels in the flat regions and relatively deep water levels along the steep hilltops.

Fig. 10 illustrates the seasonal changes of the spatial distributions of precipitation, and simulated mean LST, ET, and surface wetness, as well as root zone wetness. The observed precipitation shows obvious seasonal variations with the largest in summer (JJA) and the least in winter (DJF) (Fig. 10a). Mean LST also experiences its highest value in summer (JJA; Fig. 10b), and consequently results in the largest ET for this season Fig. 10c). Contrarily, winter (DJF) has both the lowest LST (Fig. 10b) and the least precipitation (Fig. 10a), and thus the least ET for the season (Fig. 10c). The surface soil wetness patterns are mainly determined by precipitation, bare soil evaporation, grid slope and soil pattern. Root zone wetness patterns for all seasons show good consistencies with mean deep soil wetness and the water table maps (Figs. 10e and 9). Both surface and root zone wetness show similar seasonal changes (Fig. 10d and e). The wettest surface soil and root zone occur in autumn (SON), other than summer (JJA), since autumn has much smaller ET than summer while precipitation does not decrease a lot from the summer to autumn because of typhoons and Mei-yu front activities. The driest season is in the spring (MAM) when there is relatively little precipitation but obviously increased ET (Fig. 10c) resulting from increased land surface temperature. (Fig. 10b).

Fig. 11 shows monthly water and energy cycles averaged at the upper area of the Murakami gauge from 2001 to 2004. In the sub-

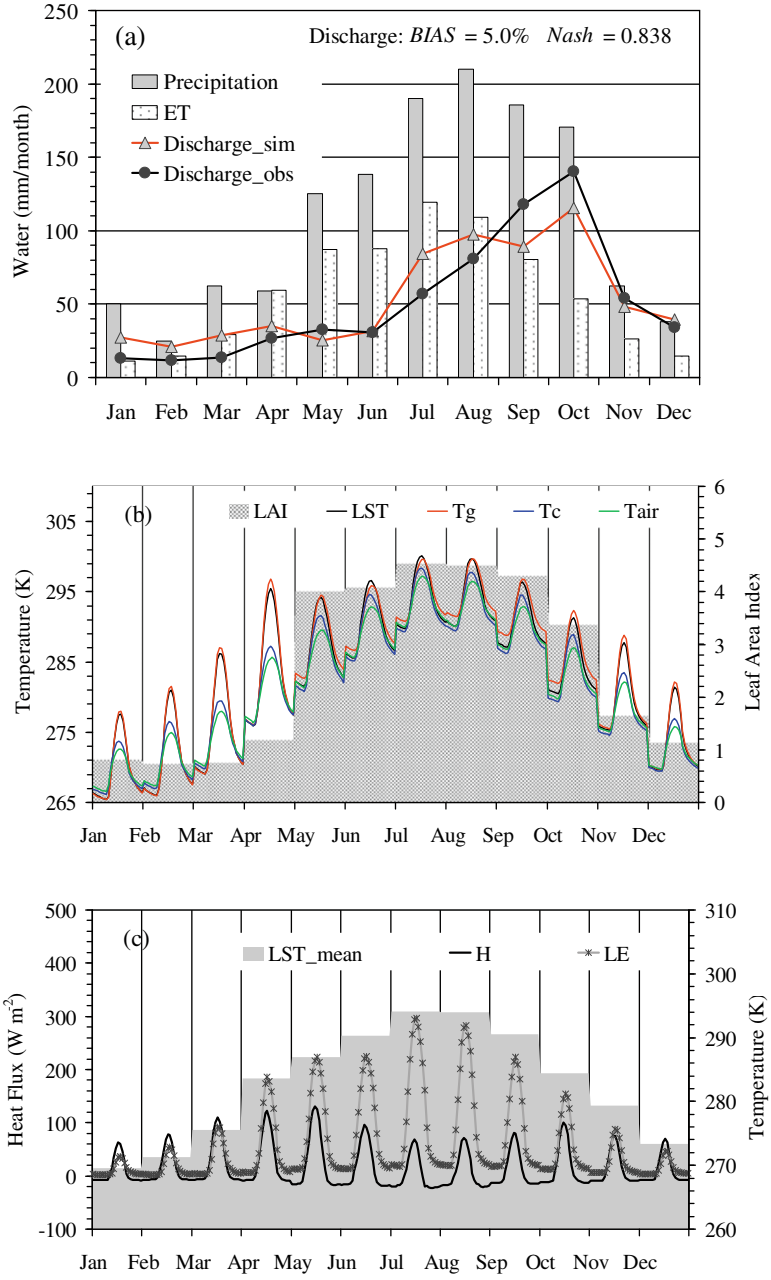

Fig. 11. Variables averaged for the upper area of the Murakami gauge from 2001 to 2004: (a) mean monthly observed discharge and precipitation, simulated discharge and ET; (b) monthly-mean LAI, as well as the diurnal variations of LST, T_g, T_c and T_{air}; and (c) mean monthly LST, and diurnal variations of sensible and latent heat fluxes (H and LE).

Please cite this article in press as: Wang, L., et al. Assessment of a distributed biosphere hydrological model against streamflow and MODIS land surface temperature in the upper Tone River Basin. J. Hydrol. (2009), doi:10.1016/j.jhydrol.2009.08.005

basin the hydrological cycles are less interfered with by reservoirs. The simulated mean monthly water balance components shows that in the sub-basin, heavy precipitation mainly occurs from May to October, months commonly associated with typhoons and Mei-yu front activities. Considering the relatively high LSTs in these months (see "LST_mean" in Fig. 11c), relatively large ETs are obtained from May to October (Fig. 11a). Monthly discharge largely concentrates during the period from July to October, and is well reproduced by WEB-DHM with the *BIAS* and *Nash* equal to 5.0% and 0.838, respectively.

Monthly mean diurnal cycles of LSTs, T_g, T_c, and T_{air} are given in Fig. 11b, and compared to the mean monthly LAI. From May to October, with relatively large LAI values, the simulated daily maximum LST is close to T_g since T_g is much greater than T_c in their peak values; while the daily minimum LST appears similar to T_c. For other months with relatively small LAI values, the diurnal cycles of LST closely follow T_g. For all months, the simulated daily minimum LST appears very close to T_{air}; while the simulated daily maximum LST is much higher than T_{air}.

Fig. 11c illustrates the mean monthly LST, as well as the diurnal variations of sensible and latent heat fluxes. The monthly changes of the daily maximum latent heat flux generally follow the monthly-mean LST with peaks in July and August. The diurnal variation of sensible heat flux is partly shaped by the diurnal change of the LST, with the largest diurnal variations in the spring (MAM).

Conclusions

In this study, a distributed biosphere hydrological model (WEB-DHM) was used to investigate the water and energy cycles in the upper Tone River Basin where flux observations are not available.

First, the model was calibrated and validated for discharges at four major stream gauges and demonstrated good performances in flood predictions, with initial soil water content before a flood event being estimated in a long-term simulation.

Second, the MODIS V5 LST products, with high resolution and reliable accuracies, were used to evaluate the model's performance in representing energy processes in the basin. The results show that the WEB-DHM reasonably accurately represents both daytime and nighttime LSTs for both time-series processes and spatial patterns, with the only calibration being for a year-long discharge at one stream gauge.

Third, basin- and sub-basin-scale water and energy cycles were analyzed and discussed. It was found that from May to October, with relatively large LAI values, the simulated daily maximum LST is close to T_g since T_g is much greater than T_c in their peak values; while the daily minimum LST appears similar to T_c. For other months with relatively small LAI values, the diurnal cycles of LST closely follow T_g .

By using a distributed hydrological model that has physically formulated water and energy budgets in the SVAT system, the recently-released MODIS V5 LST products have a big potential to improve water and energy studies for basins without flux observations (e.g., ungauged basins). This is because these tools have global coverage and high resolution.

Acknowledgements

This study was funded by Core Research for Evolutional Science and Technology, the Japan Science and Technology Corporation. Parts of this work were also support by grants from the Ministry of Education, Culture, Sports, Science and Technology of Japan, and Japan Aerospace Exploration Agency. Global 8-daily MODIS Terra Land Surface Temperature and LAI/FPAR 1 km data sets are from the EOS Data Gateway of NASA. The third author (Kun Yang) is supported by "100-Talent" Project of the Chinese Academy of Sciences.

References

Becker, F., Li, Z., 1995. Surface temperature and emissivity at various scales: Definition, measurement and related problems. Remote Sensing Reviews 12, 225–253.

Bertoldi, G., Rigon, R., Over, T.M., 2006. Impact of watershed geomorphic characteristics on the energy and water budgets. Journal of Hydrometeorology 7, 389–403.

Brown, L., Thorne, R., Woo, M.K., 2008. Using satellite imagery to validate snow distribution simulated by a hydrological model in large northern basins. Hydrological Processes 22, 2777–2787.

Crawford, T.M., Duchon, C.E., 1999. An improved parameterization for estimating effective atmospheric emissivity for use in calculating daytime downwelling longwave radiation. Journal of Applied Meteorology 38, 474–480.

Famiglietti, J.S., Wood, E.F., 1994. Multiscale modeling of spatially-variable water and energy balance processes. Water Resources Research 30, 3061–3078.

FAO, 2003. Digital Soil Map of the World and Derived Soil Properties, Land and Water Digital Media Series Rev. 1, United Nations Food and Agriculture Organization, CD-ROM.

Kerr, Y.H., Lagouarde, J.P., Imbernon, J., 1992. Accurate land surface temperature retrieval from AVHRR data with use of an improved split window algorithm. Remote Sensing of Environment 41, 197–209.

Myneni, R.B., Nemani, R.R., Running, S.W., 1997. Algorithm for the estimation of global land cover, LAI and FPAR based on radiative transfer models. IEEE Transactions on Geoscience and Remote Sensing 35, 1380–1393.

Nash, J.E., Sutcliffe, J.V., 1970. River flow forecasting through conceptual models part I – A discussion of principles. Journal of Hydrology 10 (3), 282–290.

New, M., Hulme, M., Jones, P., 2000. Representing twentieth-century space-time climate variability. Part II: Development of 1901-96 monthly grids of terrestrial surface climate. Journal of Climate 13, 2217–2238.

Norman, J.M., Becker, F., 1995. Terminology in thermal infrared remote sensing of natural surfaces. Agricultural and Forest Meteorology 77, 153–166.

O'Callaghan, J.F., Mark, D.M., 1984. The extraction of drainage networks from digital elevation data. Computer Vision, Graphics and Image Processing 28, 328–344.

Parajka, J., Bloeschl, G., 2008. The value of MODIS snow cover data in validating and calibrating conceptual hydrologic models. Journal of Hydrology 358, 240–258.

Peters-Lidard, C.D., Zion, M.S., Wood, E.F., 1997. A soil-vegetation-atmosphere transfer scheme for modeling spatially variable water and energy balance processes. Journal of Geophysical Research 102, 4303–4324.

Pinker, R.T., Sun, D., Hung, M.-P., Li, C., Basara, J.B., 2009. Evaluation of satellite estimates of land surface temperature from GOES over the United States. Journal of Applied Meteorology and Climatology 48 (1), 167–180.

Rigon, R., Bertoldi, G., Over, T.M., 2006. GEOtop: a distributed hydrological model with coupled water and energy budgets. Journal of Hydrometeorology 7, 371–388.

Sellers, P.J., Randall, D.A., Collatz, G.J., Berry, J.A., Field, C.B., Dazlich, D.A., Zhang, C., Collelo, G.D., Bounoua, L., 1996a. A revised land surface parameterization (SiB2) for atmospheric GCMs, part I: model formulation. Journal of Climate 9, 676–705.

Sellers, P.J., Los, S.O., Tucker, C.J., Justice, C.O., Dazlich, D.A., Collatz, G.J., Randall, D.A., 1996b. A revised land surface parameterization (SiB2) for atmospheric GCMs, part II: the generation of global fields of terrestrial biosphysical parameters from satellite data. Journal of Climate 9, 706–737.

Sellers, P.J., Dickinson, R.E., Randall, D.A., Betts, A.K., Hall, F.G., Berry, J.A., Collatz, G.J., Denning, A.S., Mooney, H.A., Nobre, C.A., Sato, N., Field, C.B., HendersonSellers, A., 1997. Modeling the exchanges of energy, water, and carbon between continents and the atmosphere. Science 275, 502–509.

Sheng, J.F., Wilson, J.P., Lee, S., 2009. Comparison of land surface temperature (LST) modeled with a spatially-distributed solar radiation model (SRAD) and remote sensing data. Environmental Modelling and Software 24, 436–443.

Sun, D., Pinker, R.T., 2003. Estimation of land surface temperature from a geostationary operational environmental satellite (GOES-8). Journal of Geophysical Research 108 (D11), 4326. doi:10.1029/2002JD002422.

Tang, Q., Oki, T., Kanae, S., 2006. A distributed biosphere hydrological model (DBHM) for large river basin. Annual Journal of Hydraulic Engineering – JSCE 50, 37–42.

Tarboton, D.G., Bras, R.L., Rodriguez-Iturbe, I., 1991. On the extraction of channel networks from digital elevation data. Hydrological Processes 5, 81–100.

Turner, D.P., Ritts, W.D., Cohen, W.B., Gower, S.T., Zhao, M.S., Running, S.W., Wofsy, S.C., Urbanski, S., Dunn, A.L., Munger, J.W., 2003. Scaling gross primary production (GPP) over boreal and deciduous forest landscapes in support of MODIS GPP product validation. Remote Sensing of Environment 88, 256–270.

Twine, T.E., Kucharik, C.J., 2008. Evaluating a terrestrial ecosystem model with satellite information of greenness. Journal of Geophysical Research – Biogeosciences 113, G03027. doi:10.1029/2007JG000599.

Wan, Z.M., 2008. New refinements and validation of the MODIS land-surface temperature/emissivity products. Remote Sensing of Environment 112, 59–74.

Wang, L., Koike, T., 2009. Comparison of a distributed biosphere hydrological model with GBHM. , Annual Journal of Hydraulic Engineering – JSCE 53, 103–108.

Wang, L., Koike, T., Yang, K., Jackson, T., Bindlish, R., Yang, D., 2009. Development of a distributed biosphere hydrological model and its evaluation with the

Please cite this article in press as: Wang, L., et al. Assessment of a distributed biosphere hydrological model against streamflow and MODIS land surface temperature in the upper Tone River Basin. J. Hydrol. (2009), doi:10.1016/j.jhydrol.2009.08.005

Southern Great Plains Experiments (SGP97 and SGP99). Journal of Geophysical Research – Atmospheres 114, D08107. doi:10.1029/2008JD010800.

Wigmosta, M.S., Vail, L.W., Lettenmaier, D.P., 1994. A distributed hydrology-vegetation model for complex terrain. Water Resources Research 30, 1665–1679.

Yang, D., 1998. Distributed Hydrological Model Using Hillslope Discretization Based On Catchment Area Function: Development and Applications, Ph.D. Thesis, Univ. of Tokyo, Tokyo.

Yang, D., Herath, S., Musiake, K., 2000. Comparison of different distributed hydrological models for characterization of catchment spatial variability. Hydrological Processes 14, 403–416.

Yang, K., Huang, G., Tamai, N., 2001. A hybrid model for estimating global solar radiation. Solar Energy 70, 13–22.

Yang, D., Koike, T., Tanizawa, H., 2004. Application of a distributed hydrological model and weather radar observations for flood management in the upper Tone River of Japan. Hydrological Processes 18, 3119–3132.

Yang, K., Koike, T., Ye, B., 2006. Improving estimation of hourly, daily, and monthly solar radiation by importing global data set. Agricultural and Forest Meteorology 137, 43–55.

Yin, Z.S., Williams, T.H.L., 1997. Obtaining spatial and temporal vegetation data from landsat MSS and AVHRR/NOAA satellite images for a hydrologic model. Photogrammetric Engineering and Remote Sensing 63 (1), 69–77.

Please cite this article in press as: Wang, L., et al. Assessment of a distributed biosphere hydrological model against streamflow and MODIS land surface temperature in the upper Tone River Basin. J. Hydrol. (2009), doi:10.1016/j.jhydrol.2009.08.005